Biochemical Pharmacology 208 (2023) 115410

Contents lists available at ScienceDirect

Biochemical Pharmacology

journal homepage: www.elsevier.com/locate/biochempharm

# A high-density 3-dimensional culture model of human glioblastoma for rapid screening of therapeutic resistance

J.M.C. Brown [a], M. Zaben [a,b,c], C. Ormonde [a,c], F. Sharouf [a,b,c], R. Spencer [a,b,c], H. Bhatt [b], F. A. Siebzehnrubl [d,*,1], W.P. Gray [a,b,c,*,1]

[a] Division of Psychological Medicine and Clinical Neurosciences, University Hospital Wales, Cardiff and Vale University Health Board, CF14 4XW, United Kingdom
[b] Department of Neurosurgery, University Hospital of Wales, Cardiff, United Kingdom
[c] B.R.A.I.N Biomedical Research Unit, Cardiff University, United Kingdom
[d] School of Biosciences, European Cancer Stem Cell Research Institute, Cardiff University, Cardiff CF24 4HQ, United Kingdom

ARTICLE INFO

*Keywords:*
In vitro
Preclinical models
Personalized medicine
Precision medicine

ABSTRACT

Glioblastoma is among the most lethal cancers, with no known cure. A multitude of therapeutics are being developed or in clinical trials, but currently there are no ways to predict which patient may benefit the most from which drug. Assays that allow prediction of the tumor's response to anti-cancer drugs may improve clinical decision-making. Here, we present a high-density 3D primary cell culture model for short-term testing from resected glioblastoma tissue that is set up on the day of surgery, established within 7 days and viable for at least 3 weeks. High-density 3D cultures contain tumor and host cells, including microglia, and retain key histopathological characteristics of their parent tumors, including proliferative activity, expression of the marker GFAP, and presence of giant cells. This provides a proof-of-concept that 3D primary cultures may be useful to model tumor heterogeneity. Importantly, we show that high-density 3D cultures can be used to test chemotherapy response within a 2–3-week timeframe and are predictive of patient response to Temozolomide therapy. Thus, primary high-density 3D cultures could be a useful tool for brain cancer research and prediction of therapeutic resistance.

## 1. Introduction

Glioblastoma (GBM) is the most lethal type of brain cancer in adults, with a median survival of less than 2 years using the most advanced therapies [19]. However, there are no curative therapies available, and consequently the 5-year survival rate of these cancers remains below 5 % [13]. Standard of care for most patients consists of maximum safe resection, followed by radio- and chemotherapy [2]. Many tumors show ab initio or acquired resistance against the most widely used chemotherapeutic agent, Temozolomide (Temodar®, TMZ) [22]. TMZ resistance has been linked to MGMT promoter methylation status [7], but recent evidence indicates that MGMT methylation status may not be predictive of TMZ response in all gliomas. For example, the CATNON trial found no benefit of combined TMZ and radiotherapy versus radiotherapy alone in glioblastoma, IDH wild type patients, and while MGMT methylation status was predictive of patient survival it did not predict response to TMZ [20]. The pathobiology of tumor resistance to TMZ and other chemotherapeutics has been linked to the presence of GBM cancer stem cells (CSCs) [3,18] and/or the acquisition of stem cell traits in GBM cells [8].

Molecular diagnosis is now included as part of the standard diagnostic repertoire for GBM [14], but to exploit molecular targets for individualized therapies, predictive biomarkers for sensitivity or resistance to targeted therapies are needed. Furthermore, without broad-

*Abbreviations:* CSC, Cancer stem cells; DIV, Days in vitro; DMEM, Dulbeccos' modified Eagle's medium; DMSO, Dimethyl sulfoxide; EdU, 5-ethynyl-2′-deoxyuridine; EGF, Epithelial growth factor; FGF2, Basic fibroblast growth factor; GBM, Glioblastoma; IDH1, Isocitrate dehydrogenase 1; MGMT, O6-Methylguanine-DNA Methyltransferase; OS, Overall survival; PBS, Phosphate-buffered saline; PBS-T, Phosphate-buffered saline with 0.1% Triton X-100; PFS, Progression-free survival; PTFE, Polytetrafluorethylene; TMZ, Temozolomide.

* Corresponding authors at: Division of Psychological Medicine and Clinical Neurosciences, University Hospital Wales, Cardiff and Vale University Health Board, CF14 4XW, United Kingdom (W.P. Gray).
*E-mail addresses:* fas@cardiff.ac.uk (F.A. Siebzehnrubl), graywp@cardiff.ac.uk (W.P. Gray).
[1] Equal contribution.

https://doi.org/10.1016/j.bcp.2023.115410
Received 14 October 2022; Received in revised form 30 December 2022; Accepted 3 January 2023
Available online 9 January 2023

scale, comprehensive predictive testing of therapeutic resistance or sensitivities of patient tumors, options for clinical decision-making remain limited. There is an urgent need for scalable testing that predicts therapeutic sensitivity of patient tumors in time for initiation of chemotherapy to implement more precision medicine-based approaches in clinical management of GBM.

Here, we describe a high-density 3D in vitro primary tumor tissue culture system that is established within 7 days following tumor resection surgery and that recapitulates pathological hallmarks from both the tumor and the microenvironment. These primary, high-density 3D cultures can be used to test resistance or sensitivity to chemotherapeutic agents providing a result within 2–3 weeks post-surgery, as we demonstrate with the well-known chemotherapeutic Temozolomide. We show that high-density cultures predict response to Temozolomide therapy, indicating their potential relevance to inform personalized clinical decision-making.

Our data support that the high-density culture method described here is of potential benefit for research and clinical testing, providing an accurate reflection of GBM and host cells that can provide readouts in a clinically relevant timeframe.

## 2. Material and methods

### 2.1. Reagents

MK-801 ((5R,10S)-(+)-5-methyl-10,11-dihydro-5H-dibenzo[*a*,*d*] cyclohepten-5,10-imine) maleate was purchased from Abcam (Cambridge, UK). Dispase II and DNase I were purchased from Roche (Basel, Switzerland). Papain was purchased from Merck Life Science (Gillingham, UK). PTFE confetti disc membranes were purchased from Hepia-Biosciences (Geneva, Switzerland). Paraformaldehyde was purchased from Merck Life Science (Gillingham, UK). The Click-IT EdU detection kit was purchased from Thermo Fisher Scientific (Waltham, MA USA). Antibodies were purchased from the following vendors: mouse anti b-III tubulin (TuJ1, 801202) and mouse anti CD68 (333801) from BioLegend (San Diego, CA USA), rabbit anti Iba1 (019–19741) from Fujifilm Wako (Neuss, Germany), rat anti GFAP (2.2b10, 13–0300) from Thermo Fisher Scientific (Waltham, MA USA), mouse anti IDH-1 R132H (DIA-H09) from Dianova (Hamburg, Germany), rabbit anti Nestin (ab105389) and rabbit anti Sox2 (ab97959) from Abcam (Cambridge, UK). DAPI was purchased from Merck Life Science (Gillingham, UK). Temozolomide was purchased from Tocris Bioscience (Bristol, UK).

### 2.2. Sample collection and tissue culture

GBM tumor samples were collected from patients undergoing surgical resection who gave informed consent for tissue donation through the Welsh Neuroscience Research Tissue Bank approvals process (WNRTB; Ref 19/WA/0058) and all experiments conformed to the Human Tissue Act. Suitable patients were identified by clinical staff at the University Hospital of Wales. Patient data, histological images and reports were anonymized by NHS staff. Clinical follow up data were collected by authors HB and RJS in August 2021 for the patients from whom high density 3D GBM cultures were generated. Data were collected with respect to: (i) MGMT promoter methylation status reported by neuropathology, (ii) oncological therapy received following surgical resection (concurrent temozolomide and radiotherapy followed by adjuvant temozolomide), (iii) progression-free survival (PFS) and (iv) overall survival (OS). Clinical data were analyzed using SPSS statistics 27 (IBM, Portsmouth UK).

Upon collection of tissue samples were immediately placed in 30 ml Gey's balanced salt solution (Merck Life Science, Gillingham, UK) with 10 μM (+) MK-801 maleate, on ice. Tissue samples used for successful culture generation were approximately 1 $cm^3$ in volume. Tissue samples were mechanically dissociated (McIlwain tissue chopper, Stoelting, Dublin, Ireland) and enzymatically digested (DMEM (Thermo Fisher Scientific, Waltham, MA USA), with 1 μl/ml MK-801, 1 mg/ml dispase II, 0.1 mg/ml DNase I, and 2 mg/ml papain) at 37 °C and 5 % CO2 for 45 mins. The cell solution was then strained through 100 and 40 um cell strainers (VWR, Poole, UK) to remove larger debris and obtain a single cell solution. Cells were centrifuged at 240g for 5 min and resuspended at $2.5x10^8$ cells/ml in serum-free media (96 % neurobasal A, 2 % B27, 1 % glutaMAX and 1 % penicillin/streptomycin (all from Thermo Fisher Scientific, Waltham, MA USA)). Media was added to each well of a 6 well plate (1200 μl/well). Semi-permeable well inserts (Merck Life Science, Gillingham, UK) were placed within each well, and three PTFE confetti disks added to each insert. A volume of 5 μl of cell suspension was pipetted onto each confetti disk. High-density cultures were incubated at 37 °C and 5 % CO2 throughout. Every 2–3 days, 75 % media was changed.

### 2.3. Immunofluorescence staining

High-density cultures were removed with their confetti to a 48 well plate for fixation (4 % paraformaldehyde, 30 min) and subsequent immunostaining. Cultures were fixed after 14 days in vitro (DIV) unless otherwise specified. For EdU detection, cultures were exposed to 10 μM EdU for 4 h before fixation. EdU was then detected using the Alexa-647 conjugated azide according to the manufacturer's instructions (Click-it EdU imaging kit). For immunofluorescence staining, cultures were blocked for 30 min in PBS-T with 3 % donkey serum, then incubated with primary antibodies in the same solution overnight. The following primary antibodies were used: mouse anti b-III tubulin (1:500), rabbit anti Iba1 (1:2000), rat anti GFAP (1:500), mouse anti IDH-1 R132H (1:100), rabbit anti Nestin (1:500), mouse anti CD68 (1:500), rabbit anti Sox2 (1:500). Cultures were then washed with PBS-T before incubation with appropriate secondary antibodies in 3 % donkey serum in PBS-T (1:500) for 1 h. Cultures were washed once in PBS-T then incubated with 0.5 ug/ml DAPI (4′,6-diamidino-2-phenylindole) for 5 min, followed by three further 5 min washes in PBS-T. The confetti discs were then carefully removed from their wells using tweezers and applied cell-side up to a microscope slide. A droplet of Mowiol mounting solution (Merck Life Science, Gillingham, UK) was placed on top of each culture and a cover slip was applied to the slide.

### 2.4. Temozolomide treatment

Temozolomide was applied to high-density cultures at a range of doses (5, 50, 100, 500 μM) for most samples, and a fixed dose of 100 μM to cultures obtained from regional sampling. Temozolomide was added to the media at 9 DIV. To assess cell proliferation after Temozolomide treatment, cultures were treated with EdU at 14 DIV for 4 h before fixation. EdU was detected as described above. Concentration-effect curves were generated based on the fraction of EdU-positive cells compared to DMSO treated controls using a 4-parameter logistic equation as described [9].

### 2.5. Image acquisition and data analysis

Images were taken using an upright fluorescence microscope (Leica DM6000B, Leica Microsystems, Milton Keynes, UK) or a confocal microscope (Zeiss LSM710, Carl Zeiss ltd, Cambridge, UK). Z-stack confocal images were combined into a maximum-intensity projection. Images were analyzed in ImageJ. To count DAPI + cells, a threshold filter was applied to the DAPI channel to cover visible nuclei. The watershed function was applied to separate overlapping nuclei. The 'analyse particles' function was applied to the threshold image, excluding particles smaller than 50 pixels (approximately 20 $\mu m^2$), to eliminate debris and pyknotic nuclei. Individual antibody stains were counted manually. DAPI and antibody counts were averaged from at least 4 visual fields per culture, and 5 cultures per patient.

**Table 1**
Clinical information for all patients and specimens involved in this study.

| Sample number | Age | Sex | MGMT methylation status | IDH1 mutation status | Concurrent TMZ and radiotherapy | Cycles of adjuvant TMZ | Treatment after progression | Progression-free survival | Overall Survival |
|---|---|---|---|---|---|---|---|---|---|
| GBM1 | 71 | M | M | WT | Y | 4 | Nil | 17.1 | 17.1 |
| GBM2 | 76 | F | M | WT | Y | 0 | Nil | 12.9 | 12.9 |
| GBM3 | 69 | M | Uncertain | WT | Y | 0 | Further surgery | 14.8 | 21.1 |
| GBM4 | 65 | M | M | WT | Y | 6 | TMZ | 25.5 | 30.2 |
| GBM5 | 38 | F | ND | WT | Y | 6 | PCV and carboplatin | 11.8 | 24.7 |
| GBM6 | 65 | M | M | WT | Y | 0 | Nil | 6.0 | 6.0 |
| GBM7 | 59 | M | U | WT | Y | 5 | PCV | 10.1 | 12.5 |
| GBM8 | 65 | F | M | WT | Y | 6 | TMZ | 25.2 | 46.0 |
| GBM9 | 68 | M | M | WT | Y | 6 | "Second-line" chemotherapy | 13.5 | 19.8 |
| GBM10 | 49 | M | U | WT | Y | 6 | Further surgery | 20.9 | 27.0 |
| GBM11 | 70 | M | M | WT | Missing | Missing | Missing | 7.8 | 7.8 |
| GBM12 | 77 | F | ND | WT | N | 0 | Nil | 9.3 | 9.3 |
| GBM13 | 54 | M | ND | WT | Y | 2 | Further surgery | 16.8 | 39.3 |
| GBM14 | 56 | F | U | WT | Y | 6 | Nil | 17.3 | 25.5 |
| GBM15 | 73 | M | U | WT | N | 0 | Nil | 1.2 | 1.2 |
| GBM16 | 74 | F | M | WT | Y | 6 | Nil | 42.8 | 42.8 |
| GBM18 | 48 | M | M | WT | Y | 6 | Nil | 17.3 | 20.8 |
| GBM19 | 69 | F | U | WT | Y | 3 | Nil | 6.0 | 19.4 |
| GBM20 | 62 | F | M | WT | Y | 6 | Nil | 12.6 | 14.4 |
| GBM21 | 60 | M | U | WT | Y | 3 | Nil | 13.2 | 13.2 |
| GBM22 | 60 | F | M | WT | Y | 6 | TMZ, PCV | 28.6 | 39.2 |
| GBM23 | 69 | M | M | WT | Y | 6 | Further surgery | 17.0 | 20.5 |
| GBM24 | 54 | M | M | WT | Y | 0 | Nil | 7.3 | 12.1 |
| GBM25 | 65 | M | M | WT | Y | 6 | Further surgery | 21.8 | 25.0 |
| GBM26 | 73 | M | U | WT | Y | 3 | Nil | 5.7 | 5.7 |
| GBM27 | 70 | F | U | WT | Y | 6 | Lomustine | 9.3 | 15.7 |
| GBM28 | 50 | M | M | WT | Y | 6 | Further surgery | 8.0 | 19.8 |
| GBM29 | 68 | M | M | WT | Y | 6 | Further surgery | 20.3 | 24.1 |
| GBM30 | 66 | F | M | WT | N | 0 | TMZ (initial PCV) | 23.3 | 32.4 |
| GBM31 | 50 | F | U | WT | Y | 0 | Lomustine | 22.6 | 35.2 |
| GBM32 | 65 | M | M | WT | Y | 6 | PCV | 15.1 | 20.7 |
| GBM33 | 46 | F | M | WT | Y | 6 | PCV | 10.5 | 13.3 |
| GBM34 | 60 | F | U | WT | Y | 0 | Nil | 6.3 | 12.8 |
| GBM35 | 65 | M | M | WT | Y | 4 | Nil – but on clinical trial throughout | 22.1 | 28.8 |
| GBM36 | 70 | F | U | WT | Y | 1 | TMZ | 6.5 | 18.2 |
| GBM37 | 67 | M | U | WT | Y | 5 | Lomustine | 10.0 | 11.4 |
| GBM39 | 67 | M | U | WT | Y | 0 | Nil | 4.3 | 5.1 |
| GBM40 | 52 | M | U | WT | Y | 6 | Lomustine, carboplatin | 13.2 | 20.0 |
| GBM41 | 66 | F | M | MUT | Y | 6 | Nil | 27.6 | 27.6 |
| GBM42 | 74 | M | U | WT | Y | 1 | Nil | 6.4 | 6.4 |
| GBM43 | 49 | M | U | MUT | Y | 4 | Nil | 22.4 | 27.5 |
| GBM44 | 64 | F | U | WT | Y | 4 | PCV | 13.1 | 19.0 |
| GBM45 | 54 | F | M | WT | Y | 6 | Nil | 27.3 | N/A |
| GBM46 | 66 | M | U | WT | Y | 6 | PCV | 11.1 | 21.0 |
| GBM47 | 66 | M | U | WT | Y | 6 | PCV | 9.5 | 14.2 |
| GBM48 | 65 | M | M | WT | Y | 6 | TMZ | 22.5 | N/A |
| GBM49 | 58 | F | M | WT | Y | 5 | Nil | 13.2 | 19.7 |

**Summary of clinical information**

| Variable | | Number / Median | %age of total / total range |
|---|---|---|---|
| Age (years) | | 65 | 38 – 77 (IQR 56 – 69) |
| Male sex | | 28 | 59.6% |
| MGMT promoter methylation status | Methylated | 24 | 51.1% |
| | Unmethylated | 19 | 40.4% |
| | Unknown | 4 | 8.5% |
| IDH1 mutation status | R132H mutation | 2 | 4.3% |
| | Wild-type | 45 | 95.7% |
| Concurrent TMZ and radiotherapy received | | 43 | 91.5% |
| Adjuvant TMZ (number of cycles) | 0 | 10 | 21.3% |
| | 1 | 2 | 4.3% |
| | 2 | 2 | 4.3% |
| | 3 | 3 | 6.4% |
| | 4 | 3 | 6.4% |
| | 5 | 3 | 6.4% |
| | 6 | 22 | 46.8% |
| | >6 | 1 | 2.1% |
| Progression-free survival (months) | | 13.2 | 1.2 – 42.8 (IQR 9.3 – 21.8) |
| Overall survival (months) | | 19.8 | 1.2 – 46.0 (IQR 12.9 – 27.5) |

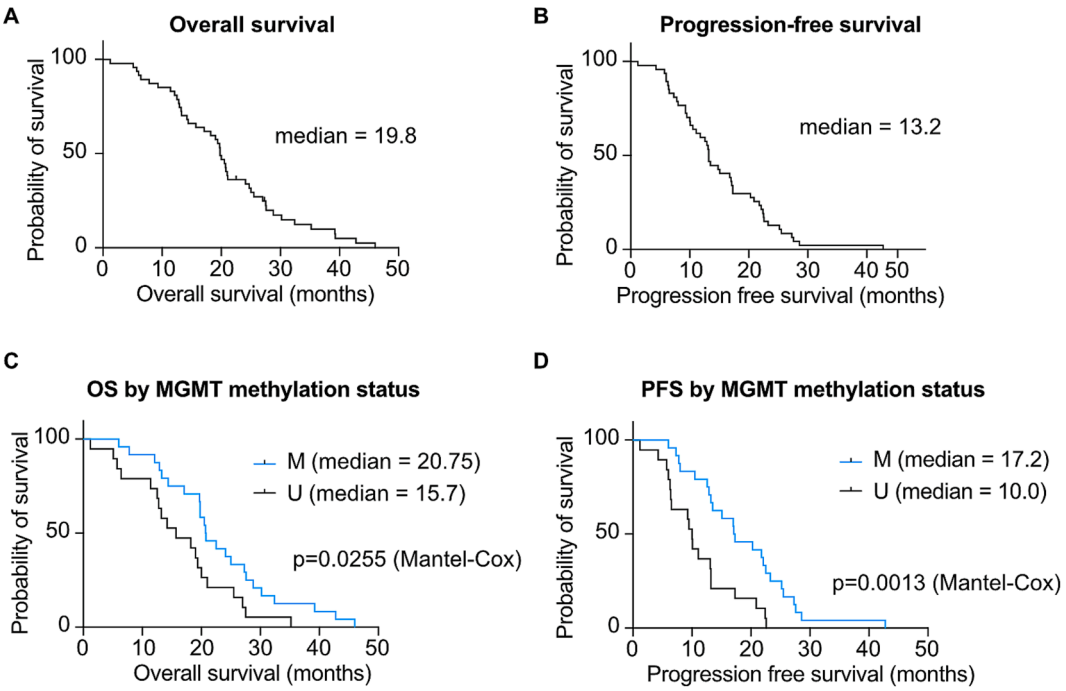


**Fig. 1. Kaplan-Meier survival curves for patients included in this study. (A)** Overall survival. **(B)** Progression-free survival. **(C)** Overall survival according to MGMT methylation status. **(D)** Progression-free survival according to MGMT methylation status. See Table 1 for patient details.

### 2.6. Statistical analysis

Statistical testing was carried out using GraphPad Prism 8 (GraphPad Software Inc., Chicago, IL USA). Unless otherwise stated, t-tests were used for comparison of two groups, and one-way ANOVA was used for comparison of three or more groups. Unless otherwise specified, data are presented as mean ± SEM.

## 3. Results

### 3.1. Patients' clinical data

High density 3D cultures were generated from tumor samples from 47 patients with a pathological diagnosis of GBM. We successfully established high density 3D cultures from all GBM patients, with cultures GBM1-GBM28 used for optimizing tissue processing, media formulation and plating density, while cultures GBM29-GBM49 were used for experiments. Cultures from 2 patients were excluded due to a final diagnosis other than GBM (metastatic disease and grade III oligodendroglioma). Full survival and progression data were available for all patients, however oncological treatment data were missing for one patient. Table 1 summarizes individual patients' data. Median age at diagnosis was 65 years (range 38 – 77) and 60 % were male.

Tumors from 24 patients (55.8 %) had methylated MGMT promoters. A total of 19 patients had unmethylated tumors and MGMT promoter methylation status was missing for 4 patients. There was no significant difference in mean age at diagnosis between methylated and unmethylated patients (*t*-test, $p = 0.453$). Two tumors were classified as grade 4 astrocytoma, IDH-mutant (R132H) [14] and the remaining 45 were grade 4 GBM, IDH-wild type. Median PFS was 13.2 months while median OS was 19.8 months (Fig. 1**A,B**). Two patients were still alive at the time of manuscript writing.

Most patients (91.5 %) received the standard of care six weeks of concurrent temozolomide (TMZ) and radiotherapy after their surgical debulking. Patients received a median of 5.5 cycles of further adjuvant TMZ. Six patients did not receive any TMZ (see Table 1 for details). Patients with methylated tumors received significantly more cycles of adjuvant TMZ than their unmethylated counterparts (median 6 vs 3 cycles, Mann-Whitney *U* test, $p = 0.027$).

In Kaplan-Meier survival analysis (Fig. 1**C,D**), the methylated group had a significant survival benefit compared to unmethylated patients in both PFS (median 17.2 vs 10 months, Mantel-Cox log rank $\chi^2 = 10.33$, $p = 0.0013$) and OS (median 20.75 vs 15.7 months, Mantel-Cox log rank $\chi^2 = 4.989$, $p = 0.0255$).

### 3.2. Characterization of high-density 3D cultures from human GBM

To establish an in vitro system that contains GBM cells as well as local microenvironmental cells and that is suitable for screening tumor cell response to therapeutics in a short timeframe, we adapted a method that we previously established in primary human hippocampal cultures [23]. To generate high-density cultures, for each culture 5 µl of a single cell suspension of primary GBM cells at a density of $2.5 \times 10^8$ cells/ml were plated on a PTFE membrane. High-density cultures were grown at the media-air interface using a defined serum-free medium without additional mitogens (e.g., EGF, FGF2; Fig. 2**A,B**). High-density cultures show an initial consolidation phase over the first week in culture that is characterized by a significant decrease in cell numbers, followed by a stable culture period thereafter with no significant changes in cell numbers between time points (Fig. 2**C**). Likewise, the labelling index of cell proliferation in the high-density cultures (i.e., cell cycle rate), defined by the ratio of EdU + Ki67 + over total Ki67 + cells, remains stable over the culture period. A significantly lower labelling index at 21 days in culture could indicate eventual decrease of proliferation rates (Fig. 2**D**). Thus, high-density cultures are established at the day of surgery and have consolidated into a usable in vitro system within 7 days after patient resection.

We next characterized the cell types present in high-density cultures. To conclusively label tumor cells within high density cultures, we exploited the IDH1 mutation which is typically shared in > 95 % of tumor cells as it occurs early during tumorigenesis [5]. We selected a patient with IDH1-mutant (R132H) astrocytoma to assess the prevalence of tumor cells in high-density cultures (Fig. 2**E**).

R132H staining confirmed presence of tumor cells, but also showed a

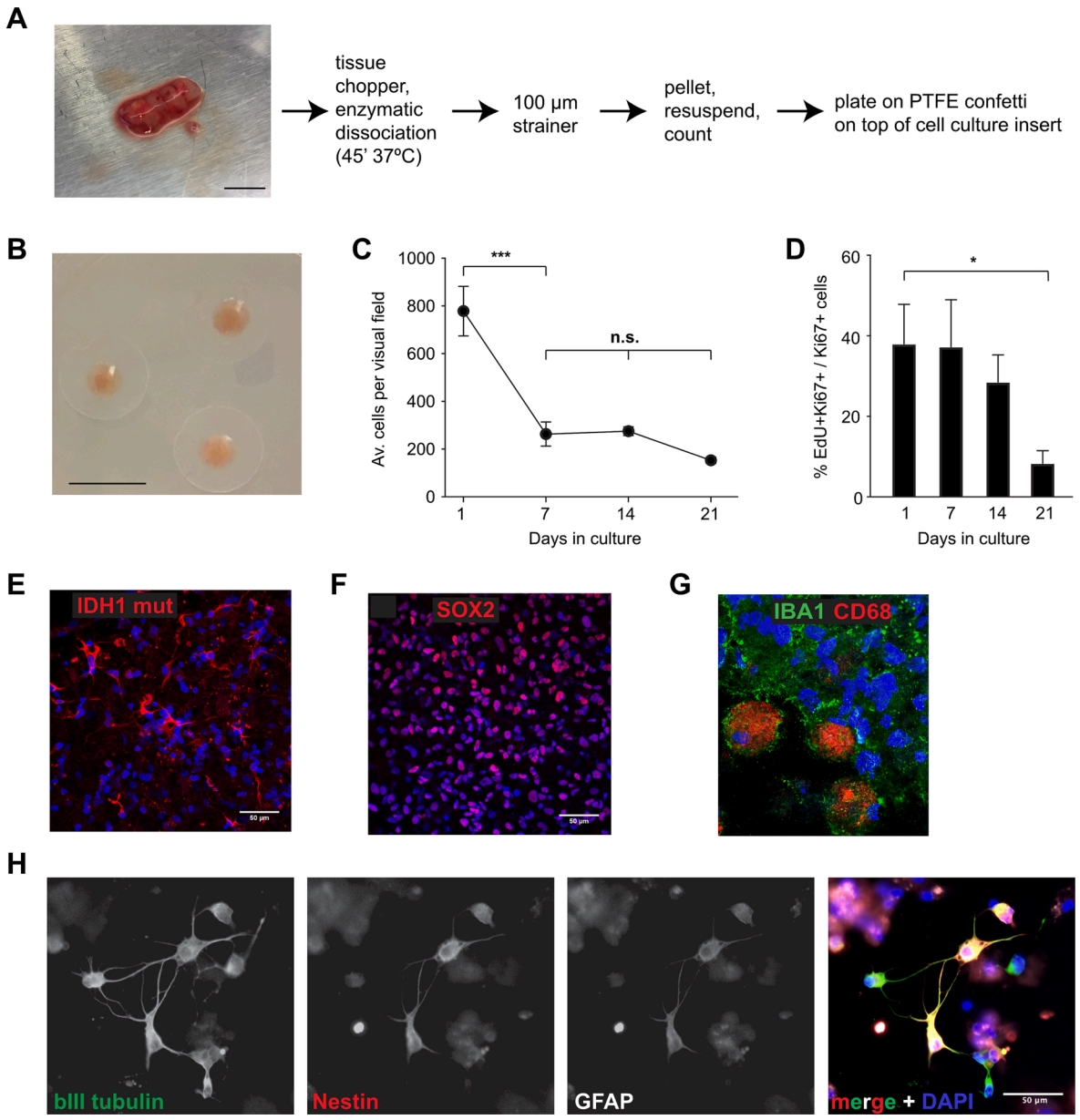


**Fig. 2. Characterization of high-density cultures. (A)** Schematic of human high-density culture preparation. Tissue from surgical resections (left image) is mechanically and enzymatically dissociated, passed through a 100 µm strainer to remove debris, and centrifuged before plating a defined number of cells (see Material and Methods) onto a PTFE membrane placed on top of a cell culture insert at the liquid–air interface. Scale bar 1 cm. **(B)** Image shows 3 established high-density cultures on top of PTFE membranes. Scale bar 5 mm. **(C)** After an initial consolidation phase (day 1–7), the number of cells within high-density cultures remain stable over at least 3 weeks (n = 3 patient cultures with 5 replicates per time point; *** $p < 0.001$, n.s. not significant). **(D)** Labelling index shows active and stable proliferation within high-density cultures over 2 weeks that eventually slows around 3 weeks after plating (n = 3 patient cultures with 5 replicates per time point; * $p < 0.05$). **(E)** Immunofluorescence staining for IDH1-R132H demonstrates that high-density cultures contain both tumor and non-tumor cells. Scale bar 50 µm. **(F)** Immunofluorescence staining for SOX2 highlights presence of cancer stem cells in high-density cultures. Scale bar 50 µm. **(G)** Immunofluorescence staining confirmed presence of microglia (IBA1) of different activation states (CD68) in high-density cultures. **(H)** GBM cells in high-density cultures frequently co-express neuronal (bIII tubulin), progenitor (Nestin) and astrocytic (GFAP) markers. Scale bar 50 µm (applies to all images).

significant fraction of non-tumor cells in high-density cultures. We further evaluated tumor and non-tumor cell populations in high density cultures in IDH wild type GBM patients. To assess the presence of GBM cancer stem cells we used immunofluorescence staining for the cancer stem cell marker SOX2 (Fig. 2**F**). To evaluate non-tumor cell populations in high-density cultures we focused on microglia, which constitute the most frequent cell type within GBM [10]. Co-staining for IBA1 and CD68 demonstrated presence of microglia in high-density cultures and revealed heterogeneity of microglial activation stages (Fig. 2**G**). To further characterize GBM cells within high-density cultures, we co-stained for the early neuronal marker tubulin beta III (TuJ1), the stem/progenitor marker Nestin and the astrocyte marker GFAP (Fig. 2**H**). Most GBM cells expressed all three markers, although there was some heterogeneity among the intensity of individual marker expression.

Our findings show that high-density 3D cultures can be established within 7 days of surgical resection, are viable over at least 3 weeks, and contain tumor and non-tumor cells.

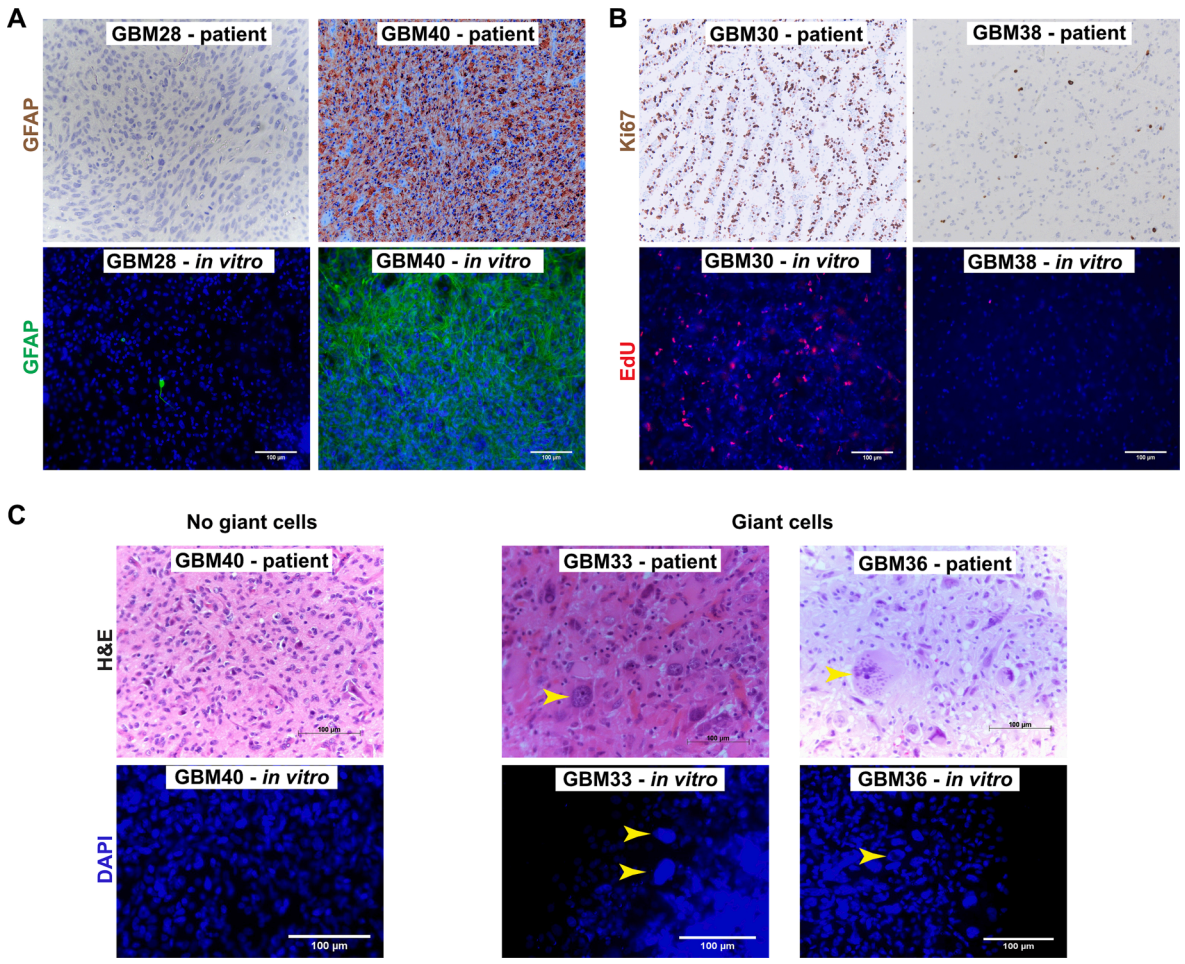


**Fig. 3. High-density cultures share neuropathological features of parent tumors.** Established high-density cultures retain histopathological hallmarks of parent tumors, including immunoreactivity for GFAP **(A)**, frequency of proliferating cells **(B)** and the presence of giant cells **(C)**. Depicted are representative images of parental tumors (top row) and the corresponding high-density cultures (bottom row). Arrowheads indicate giant cells. Scale bars 100 µm.

**Table 2**
Comparison of high-density 3D cultures and patient pathological features.

| Sample | Ki-67 pathology | Pathology results | Culture EdU count |
|---|---|---|---|
| GBM30 | Up to 50 % | HIGH | 1299 |
| GBM31 | <1% | LOW | 355 |
| GBM33 | 60 % | HIGH | 1507 |
| GBM34 | 20 % | MED | 98 |
| GBM37 | 20–25 % | MED | 192 |
| GBM39 | 40 % | HIGH | 1335 |
| GBM43 | Low, but areas of 20–40 % | LOW | NA |
| GBM44 | 30 % | MED | 60 |
| GBM45 | 30 % | MED | 54 |
| GBM46 | Up to 25 % | MED | 87 |
| GBM47 | Up to 30 % | MED | 212 |
| GBM48 | 40 % | HIGH | NA |
| GBM49 | 25 % | MED | 22 |

### *3.3. Comparison of high-density cultures with parent tumor histopathology*

Next, we determined to which degree high-density cultures share cellular morphology phenotypes with the original patient tumor. For this, we compared immunohistochemistry and H&E staining of patient material taken for histopathological diagnosis with immunofluorescence staining of high-density cultures. We found that high-density cultures expressed histopathological marker GFAP at similar levels as their parent tumors (Fig. 3**A**). High-density cultures also showed EdU uptake at comparable levels to proliferation levels in their parent tumors (Fig. 3**B**, Table 2). The presence of giant cells is a hallmark of a subgroup of GBMs [14], a finding which was mirrored in high-density cultures. Cultures from 3 patients where giant cells were confirmed by histopathology showed giant nuclei as well. High-density cultures from 12 patients where no giant cells were detected in material sent for neuropathological diagnosis did not contain giant cells (Fig. 3**C**).

Together, this shows that high-density cultures share at least some cellular morphology phenotypes with their parent tumors. We next asked whether high-density cultures also reflect treatment response of patient tumors.

### *3.4. High-density 3D cultures exhibit chemoresistance profiles of parent tumors and predict patient response to chemotherapy*

Because high-density cultures shared histopathological features with the patient material, we wanted to determine whether these cultures could also mirror treatment response characteristics of their parent tumors, and whether these cultures could be used to predict response to chemotherapy. Therefore, we assessed cellular response of high-density cultures after exposure to increasing concentrations of the standard chemotherapeutic TMZ compared to DMSO-treated controls by quantifying short-term EdU incorporation (Fig. 4**A**), which is proportional to proliferation rates. Experimenters conducting dose–response testing of TMZ were blinded to the neuropathological and MGMT promoter methylation-status of the parent tumors. We noted that some high-density cultures were sensitive to TMZ, with an $IC_{50}$ of EdU

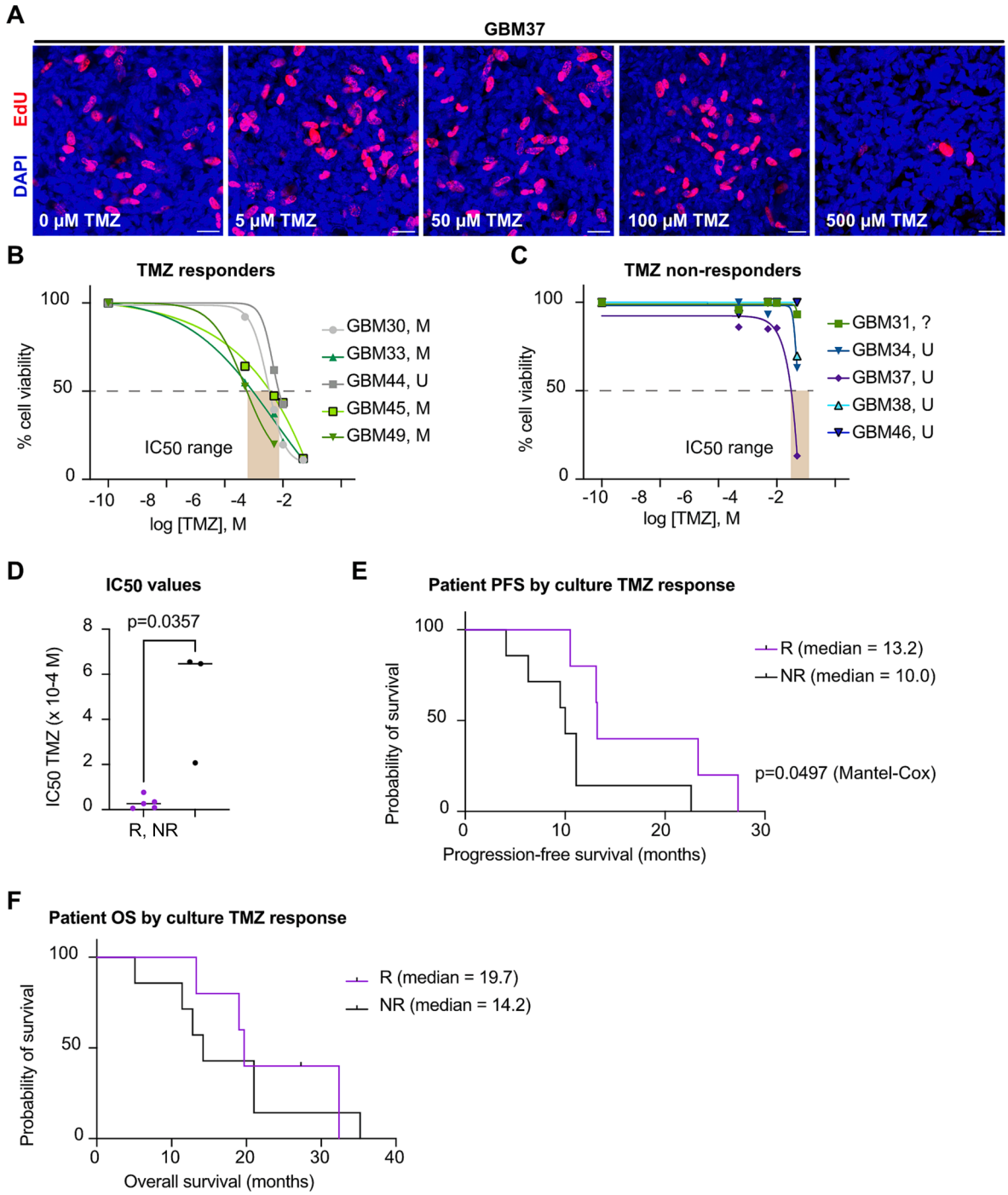


**Fig. 4. Chemoresistance profiles of high-density cultures. (A)** Representative images of short-term EdU incorporation in a GBM patient culture across a range of TMZ concentrations. All scale bars 20 µm. **(B,C)** Cell proliferation rates based on short-term EdU incorporation of high-density cultures after Temozolomide (TMZ) treatment reflects patient MGMT methylation status (**B**, TMZ sensitive cultures; **C**, TMZ resistant cultures; n = 5 replicates per culture; greyed area indicates $IC_{50}$ concentration ranges). TMZ resistance correlates with MGMT promoter methylation status of parental tumor (M: methylated, U: unmethylated, ?: unknown). **(D)** Comparison of $IC_{50}$ values from TMZ-sensitive (responding, R) and TMZ-resistant (non-responding, nR) cultures. Data points for nR cultures GBM31 and GBM46 are missing because no $IC_{50}$ values could be calculated due to the high TMZ resistance of these cultures. **(E)** Progression-free survival of patients stratified according to high-density culture response (responding: R.; non-responding: NR). **(F)** Overall survival of patients stratified according to high-density culture response (responding: R.; non-responding: NR).

incorporation in the µM range (Fig. 4**B**), whereas other cultures showed TMZ resistance with mM $IC_{50}$ (Fig. 4**C**). We were able to establish whether a culture was TMZ sensitive or resistant within 14 days of surgical tumor resection.

When comparing TMZ responses of high-density cultures post-hoc with MGMT promoter methylation status, we found that TMZ sensitive cultures were almost exclusively derived from patients with MGMT promoter methylation, whereas TMZ resistant cultures were mostly derived from patients with unmethylated MGMT promoters (Fig. 4**B,C**). MGMT promoter methylation is frequently associated with a hypermethylated phenotype (G-CIMP) in GBM [4] and with prolonged survival in patients treated with TMZ [1]. Statistical analysis of $IC_{50}$

values from TMZ sensitive (responding, R) versus TMZ resistant (non-responding, NR) cultures revealed a significant difference (Fig. 4**D**; $p = 0.0357$, Mann-Whitney test).

We next compared the response of high-density cultures with patient outcomes. When patients were stratified according to TMZ response of their corresponding high-density cultures, we found a significant difference in progression-free survival of patients with TMZ-sensitive cultures (responding, R) compared to patients with TMZ-resistant cultures (non-responding, NR) (Fig. 4**E**). This may indicate that patient tumors with TMZ-sensitive cultures showed better response to this chemotherapeutic agent than tumors from patients with TMZ resistant cultures. Of note, we did not find a significant difference in overall survival of patients stratified according to TMZ response of their corresponding high-density cultures (Fig. 4**F**), indicating that high-density cultures are more predictive of immediate response of patient tumors rather than long-term outcomes. This demonstrates a predictive effect of high-density culture sensitivity, established within 14 days of resection, on patient progression-free survival.

## 4. Discussion

There is an urgent need to improve clinical management of patients with GBM. Incredible progress has been made over the last 2–3 decades in understanding molecular determinants of GBM tumor development and progression [4,6,21], as well as the cellular and molecular basis of the heterogeneity of this disease [15,16]. But so far, little of this progress has been successfully translated into new therapies. The profound heterogeneity of GBM has highlighted that it is unlikely that there will be a 'one-size-fits-all' therapy, and some degree of individualized treatment that is somehow tailored to the patient's tumor is likely to be necessary.

The method described here allows generating hundreds of high-density cultures from an individual patient simultaneously and within 1–2 weeks following surgical resection of tissue. The number of parallel cultures as well as the short timeframe for establishing these cultures positions this system exquisitely for rapid clinical testing of drug sensitivities as shown here. We demonstrate proof-of-concept that a biological readout of TMZ resistance can be obtained within 2–3 weeks after surgery and is predictive of patient response to TMZ chemotherapy as evaluated by PFS. TMZ resistance patterns in high-density cultures from patient tumors complemented standard molecular pathology MGMT promoter methylation testing. While there was no perfect correlation, in most patients MGMT methylation status agreed with TMZ sensitivity. Since MGMT methylation is not predictive in all high-grade gliomas [20], additional methods that predict tumor response to chemotherapy could help close a gap in clinical decision making.

In addition to similar molecular characteristics, established high-density cultures exhibited cellular and histopathological hallmarks of parent tumors, including GFAP expression, proliferation, and the presence of giant cells. These features render high-density cultures a potentially useful tool to study tumor pathology and biology. Additionally, the presence of key immune cells such as microglia, as well as GBM cancer stem-like cells within high-density cultures indicates their potential for reflecting critical cell–cell interactions in the tumor microenvironment. Therefore, high-density cultures may prove valuable in both research and clinical settings. The rapid set-up and short-term readout from these cultures further enables their broad application across many settings.

The high-density cultures comprise a 3D short-term tissue culture model that includes both GBM and TME immune components. Thus, high-density cultures reflect TME elements that conventional cell culture models and some animal models are missing (e.g., xenograft models lacking immune components) [17]. Genetically engineered mouse models of GBM allow orthotopic tumor initiation and progression within a fully intact TME but rely on a defined set of mutations driving tumor growth that only incompletely reflect the diverse and heterogeneous mutational landscape of these cancers [17]. By contrast, patient-derived xenograft (PDX) models are considered the current gold standard in oncology research and for predicting response to therapy [12]. While these models are closer to recapitulating a TME than conventional subcutaneous xenograft models, they are technically demanding, and require immune suppression to prevent graft rejection. Hence, PDX models critically lack immune cell components which can influence cancer progression and response to therapy. PDX models are also not readily amenable to medium–high throughput investigations, given the overall technical challenges that PDX models present. Additionally, the growth rates of GBM mouse models limit their usefulness for predicting individual responses in patients (precision medicine) within a clinically relevant timeframe. These issues further emphasize the need for immune competent GBM models, which fully recapitulate interactions between human tumor cells and the surrounding normal human brain environment. Many contemporary 3D models rely on co-culturing patient derived GBM cells with TME components derived from pluripotent stem cells (e.g., hiPSC), but these will lack a TME that has been educated by the patient tumor. A recent landmark study demonstrated that GBM organoids can be generated and used in a similar timeframe as the high-density cultures described here [11]. Thus, our work extends the available experimental toolbox for rapid establishment of GBM cultures that reflect essential hallmarks of the patient tumor, and which are suitable for clinically relevant assays to predict patient response to therapy.

We present a method for primary 3D cultures of GBM tissue that can provide a rapid readout of drug sensitivity. Currently, our findings are limited by the number of patients analyzed, but even in the small cohort available we showed a predictive value of high-density 3D cultures. Furthermore, molecular genetic profiling of primary cell cultures and parent tumors could provide important validation that primary cultures reflect molecular subclasses of parent tumors.

In summary, we describe a rapid and simple method for generating high-density cultures from patient GBM tissue that is amenable to clinical and research settings, allows capturing regional heterogeneity and is predictive of patient therapy response.

## CRediT authorship contribution statement

**J. Brown:** Data curation, Formal analysis, Investigation, Methodology, Writing – original draft. **M. Zaben:** Supervision, Methodology, Writing – review & editing. **C. Ormonde:** Data curation, Validation. **F. Sharouf:** Data curation, Validation. **R. Spencer:** Data curation, Validation. **H. Bhatt:** Data curation, Validation. **F.A. Siebzehnrubl:** Supervision, Methodology, Funding acquisition, Writing – original draft, Writing – review & editing. **W.P. Gray:** Supervision, Methodology, Funding acquisition, Writing – review & editing.

## Declaration of Competing Interest

The authors declare that they have no known competing financial interests or personal relationships that could have appeared to influence the work reported in this paper.

## Data availability

Data will be made available on request.

## Acknowledgements

The authors would like to thank members of the WPG and FAS labs for critical comments on the manuscript. WPG is funded by NC3Rs project NC/N002423/1. FAS is supported by MRC grant MR/S007709/1. The BRAIN Unit is funded by Welsh Government through Health and Care Research Wales (BRAIN Unit Infrastructure Award, Grant no: UA05 to WPG).

## References


[1] K. Aldape, G. Zadeh, S. Mansouri, G. Reifenberger, A. von Deimling, Glioblastoma: pathology, molecular mechanisms and markers, Acta Neuropathol. 129 (2015) 829–848, https://doi.org/10.1007/s00401-015-1432-1.

[2] B.M. Alexander, T.F. Cloughesy, Adult Glioblastoma, J. Clin. Oncol. 35 (2017) 2402–2409, https://doi.org/10.1200/JCO.2017.73.0119.

[3] S. Bao, Q. Wu, R.E. McLendon, Y. Hao, Q. Shi, A.B. Hjelmeland, M.W. Dewhirst, D. D. Bigner, J.N. Rich, Glioma stem cells promote radioresistance by preferential activation of the DNA damage response, Nature 444 (2006) 756–760.

[4] C.W. Brennan, R.G. Verhaak, A. McKenna, B. Campos, H. Noushmehr, S.R. Salama, S. Zheng, D. Chakravarty, J.Z. Sanborn, S.H. Berman, et al., The somatic genomic landscape of glioblastoma, Cell 155 (2013) 462–477, https://doi.org/10.1016/j.cell.2013.09.034.

[5] D. Capper, H. Zentgraf, J. Balss, C. Hartmann, A. von Deimling, Monoclonal antibody specific for IDH1 R132H mutation, Acta Neuropathol. 118 (2009) 599–601, https://doi.org/10.1007/s00401-009-0595-z.

[6] M. Ceccarelli, F.P. Barthel, T.M. Malta, T.S. Sabedot, S.R. Salama, B.A. Murray, O. Morozova, Y. Newton, A. Radenbaugh, S.M. Pagnotta, et al., Molecular Profiling Reveals Biologically Discrete Subsets and Pathways of Progression in Diffuse Glioma, Cell 164 (2016) 550–563, https://doi.org/10.1016/j.cell.2015.12.028.

[7] S.E. Combs, S. Rieken, W. Wick, A. Abdollahi, A. von Deimling, J. Debus, C. Hartmann, Prognostic significance of IDH-1 and MGMT in patients with glioblastoma: One step forward, and one step back? Radiat. Oncol. 6 (2011) 115, https://doi.org/10.1186/1748-717X-6-115.

[8] A. Dirkse, A. Golebiewska, T. Buder, P.V. Nazarov, A. Muller, S. Poovathingal, N.H. C. Brons, S. Leite, N. Sauvageot, D. Sarkisjan, et al., Stem cell-associated heterogeneity in Glioblastoma results from intrinsic tumor plasticity shaped by the microenvironment, Nat. Commun. 10 (2019) 1787, https://doi.org/10.1038/s41467-019-09853-z.

[9] I.Y. Eyupoglu, E. Hahnen, R. Buslei, F.A. Siebzehnrubl, N.E. Savaskan, M. Luders, C. Trankle, W. Wick, M. Weller, R. Fahlbusch, I. Blumcke, Suberoylanilide hydroxamic acid (SAHA) has potent anti-glioma properties in vitro, ex vivo and in vivo, J. Neurochem. 93 (2005) 992–999.

[10] R. Glass, M. Synowitz, CNS macrophages and peripheral myeloid cells in brain tumours, Acta Neuropathol. 128 (2014) 347–362, https://doi.org/10.1007/s00401-014-1274-2.

[11] F. Jacob, R.D. Salinas, D.Y. Zhang, P.T.T. Nguyen, J.G. Schnoll, S.Z.H. Wong, R. Thokala, S. Sheikh, D. Saxena, S. Prokop, et al., A Patient-Derived Glioblastoma Organoid Model and Biobank Recapitulates Inter- and Intra-tumoral Heterogeneity, Cell 180 (188–204) (2020) e122.

[12] Y. Koga, A. Ochiai, Systematic Review of Patient-Derived Xenograft Models for Preclinical Studies of Anti-Cancer Drugs in Solid Tumors, Cells 8 (2019), https://doi.org/10.3390/cells8050418.

[13] D. Krex, B. Klink, C. Hartmann, A. von Deimling, T. Pietsch, M. Simon, M. Sabel, J. P. Steinbach, O. Heese, G. Reifenberger, et al., Long-term survival with glioblastoma multiforme, Brain J. Neurol. 130 (2007) 2596–2606, https://doi.org/10.1093/brain/awm204.

[14] D.N. Louis, A. Perry, P. Wesseling, D.J. Brat, I.A. Cree, D. Figarella-Branger, C. Hawkins, H.K. Ng, S.M. Pfister, G. Reifenberger, et al., The 2021 WHO Classification of Tumors of the Central Nervous System: a summary, Neuro Oncol. 23 (2021) 1231–1251, https://doi.org/10.1093/neuonc/noab106.

[15] C. Neftel, J. Laffy, M.G. Filbin, T. Hara, M.E. Shore, G.J. Rahme, A.R. Richman, D. Silverbush, M.L. Shaw, C.M. Hebert, et al., An Integrative Model of Cellular States, Plasticity, and Genetics for Glioblastoma, Cell 178 (835–849) (2019) e821.

[16] A.P. Patel, I. Tirosh, J.J. Trombetta, A.K. Shalek, S.M. Gillespie, H. Wakimoto, D. P. Cahill, B.V. Nahed, W.T. Curry, R.L. Martuza, et al., Single-cell RNA-seq highlights intratumoral heterogeneity in primary glioblastoma, Science 344 (2014) 1396–1401, https://doi.org/10.1126/science.1254257.

[17] F.L. Robertson, M.A. Marques-Torrejon, G.M. Morrison, S.M. Pollard, Experimental models and tools to tackle glioblastoma, Dis. Model. Mech. 12 (2019), https://doi.org/10.1242/dmm.040386.

[18] F.A. Siebzehnrubl, D.J. Silver, B. Tugertimur, L.P. Deleyrolle, D. Siebzehnrubl, M. R. Sarkisian, K.G. Devers, A.T. Yachnis, M.D. Kupper, D. Neal, et al., The ZEB1 pathway links glioblastoma initiation, invasion and chemoresistance, EMBO Mol. Med. 5 (2013) 1196–1212, https://doi.org/10.1002/emmm.201302827.

[19] R. Stupp, S. Taillibert, A.A. Kanner, S. Kesari, D.M. Steinberg, S.A. Toms, L. P. Taylor, F. Lieberman, A. Silvani, K.L. Fink, et al., Maintenance Therapy With Tumor-Treating Fields Plus Temozolomide vs Temozolomide Alone for Glioblastoma: A Randomized Clinical Trial, J. Am. Med. Assoc. 314 (2015) 2535–2543, https://doi.org/10.1001/jama.2015.16669.

[20] C.M.S. Tesileanu, M. Sanson, W. Wick, A.A. Brandes, P.M. Clement, S.C. Erridge, M.A. Vogelbaum, A.K. Nowak, J.F. Baurain, W.P. Mason, et al., Temozolomide and Radiotherapy versus Radiotherapy Alone in Patients with Glioblastoma, IDH-wildtype: Post Hoc Analysis of the EORTC Randomized Phase III CATNON Trial, Clin. Cancer Res. 28 (2022) 2527–2535, https://doi.org/10.1158/1078-0432.CCR-21-4283.

[21] R.G. Verhaak, K.A. Hoadley, E. Purdom, V. Wang, Y. Qi, M.D. Wilkerson, C. R. Miller, L. Ding, T. Golub, J.P. Mesirov, et al., Integrated genomic analysis identifies clinically relevant subtypes of glioblastoma characterized by abnormalities in PDGFRA, IDH1, EGFR, and NF1, Cancer Cell 17 (2010) 98–110. S1535-6108(09)00432-2 [pii]10.1016/j.ccr.2009.12.020.

[22] M. Weller, R. Stupp, G. Reifenberger, A.A. Brandes, M.J. van den Bent, W. Wick, M. E. Hegi, MGMT promoter methylation in malignant gliomas: ready for personalized medicine? Nat. Rev. Neurol. 6 (2010) 39–51, https://doi.org/10.1038/nrneurol.2009.197.

[23] M. Zaben, N. Haan, F. Sharouf, A. Ahmed, L.E. Sundstrom, W.P. Gray, IL-1beta and HMGB1 are anti-neurogenic to endogenous neural stem cells in the sclerotic epileptic human hippocampus, J. Neuroinflammation 18 (2021) 218, https://doi.org/10.1186/s12974-021-02265-1.